Polarization control using passive and active crossed graphene gratings

JIAN WEI YOU[1] AND NICOLAE C. PANOIU[1,*]

[1]*Department of Electronic and Electrical Engineering,University College London, Torrington Place, London WC1E 7JE, United Kingdom*

[*]n.panoiu@ucl.ac.uk

Abstract: Graphene gratings provide a promising route towards the miniaturization of THz metasurfaces and other photonic devices, chiefly due to remarkable optical properties of graphene. In this paper, we propose novel graphene nanostructures for passive and active control of the polarization state of THz waves. The proposed devices are composed of two crossed graphene gratings separated by an insulator spacer. Because of specific linear and nonlinear properties of graphene, these optical metasurfaces can be utilized as ultrathin polarization converters operating in the THz frequency domain. In particular, our study shows that properly designed graphene polarizers can effectively select specific polarization states, their thickness being about a tenth of the operating wavelength and size more than 80× smaller than that of similar metallic devices. Equally important, we demonstrate that the nonlinear optical properties of graphene can be utilized to actively control the polarization state of generated higher harmonics.

© 2018 Optical Society of America

References and links

1. K. S. Novoselov, A. K. Geim, S. V. Morozov, D. Jiang, Y. Zhang, S. V. Dubonos, I. V. Grigorieva, and A. A. Firsov, "Electric field effect in atomically thin carbon films," Science **306**(5696), 666–669 (2004).
2. K. I. Bolotin, K. J. Sikes, Z. Jiang, M. Klima, G. Fudenberg, J. Hone, P. Kim, and H. L. Stormer, "Ultrahigh electron mobility in suspended graphene," Solid State Commun. **146**(9), 351–355 (2008).
3. F. Bonaccorso, Z. Sun, T. Hasan, A. C. Ferrari, "Graphene photonics and optoelectronics," Nat. Photonics **4**(9), 611–622 (2010).
4. K. S. Novoselov, V. I. Fal, L. Colombo, P. R. Gellert, M. G. Schwab, and K. Kim, "A roadmap for graphene," Nature **490**(7419),192–200 (2012).
5. A. K. Geim, "Graphene: status and prospects," Science **324**(5934), 1530–1534 (2009).
6. F. Schwierz, "Graphene transistors," Nat. Nanotechnol. **5**(7), 487–496 (2010).
7. Y. M. Lin, C. Dimitrakopoulos, K. A. Jenkins, D. B. Farmer, H. Y. Chiu, A. Grill, and P. Avouris, "100-GHz transistors from wafer-scale epitaxial graphene," Science **327**(5966), 662–662 (2010).
8. G. S. Kulkarni, K. Reddy, Z. Zhong, and X. Fan, "Graphene nanoelectronic heterodyne sensor for rapid and sensitive vapour detection," Nat. Commun. **5**, 4376 (2014).
9. M. Zhong, D. Xu, X. Yu, K. Huang, X. Liu, Y. Qu, Y. Xu, and D. Yang , "Interface coupling in graphene/fluorographene heterostructure for high-performance graphene/silicon solar cells," Nano Energy **28**, 12–18 (2016).
10. S. Y. Hong, J. I. Dadap, N. Petrone, P. C. Yeh, J. Hone, and R. M. Osgood Jr, "Optical third-harmonic generation in graphene," Phys. Rev. X **3**(2), 021014 (2013).
11. J. L. Cheng, N. Vermeulen, and J. E. Sipe, "Third order optical nonlinearity of graphene," New J. Phys. **16**(5), 053014 (2014).
12. J. D. Cox, I. Silveiro and F. J. G. de Abajo, "Quantum effects in the nonlinear response of graphene plasmons," ACS Nano **10**(2), 1995–2003 (2016).
13. J. W. You, J. You, M. Weismann, and N. C. Panoiu, "Double-resonant enhancement of third-harmonic generation in graphene nanostructures," Phil. Trans. R. Soc. A **375**(2090), 20160313 (2017).
14. H. Zhang, S. Virally, Q. Bao, L. K. Ping, S. Massar, N. Godbout, and P. Kockaert, "Z-scan measurement of the nonlinear refractive index of graphene," Opt. Lett. **37**(11), 1856–1858 (2012).
15. G. K. Lim, Z. L. Chen, J. Clark, R. G. Goh, W. H. Ng, H. W. Tan, R. H. Friend, P. K. Ho, and L. L. Chua, "Giant broadband nonlinear optical absorption response in dispersed graphene single sheets," Nat. Photonics **5**(9), 554–560 (2011).
16. G. W. Hanson, "Dyadic Green's functions and guided surface waves for a surface conductivity model of graphene," J. Appl. Phys. **103**(6), 064302 (2008).
17. P. A. D. Goncalves and N. M. Peres, *An introduction to graphene plasmonics* (World Scientific, 2016).

18. H. Choi, F. Borondics, D. A. Siegel, S. Y. Zhou, M. C. Martin, A. Lanzara, and R. A. Kaindl, "Broadband electromagnetic response and ultrafast dynamics of few-layer epitaxial graphene," Appl. Phys. Lett. **94**(17), 172102 (2009).

19. J. M. Dawlaty, S. Shivaraman, J. Strait, P. George, M. Chandrashekhar, F. Rana, M. G. Spencer, D. Veksler, and Y. Chen, "Measurement of the optical absorption spectra of epitaxial graphene from terahertz to visible," Appl. Phys. Lett. **93**(13), 131905 (2008).

20. S. Winnerl, M. Orlita, P. Plochocka, P. Kossacki, M. Potemski, T. Winzer, E. Malic, A. Knorr, M. Sprinkle, C. Berger, and W. A. De Heer, "Carrier relaxation in epitaxial graphene photoexcited near the Dirac point," Phys. Rev. Lett. **107**(23), 237401 (2011).

21. L. Ju, B. Geng, J. Horng, C. Girit, M. Martin, Z. Hao, H. A. Bechtel, X. Liang, A. Zettl, Y. R. Shen, and F. Wang, "Graphene plasmonics for tunable terahertz metamaterials," Nat. Nanotechnol. **6**(10), 630–634 (2011).

22. P. A. D. Goncalves, E. J. C. Dias, Y. V. Bludov, and N. M. R. Peres, "Modeling the excitation of graphene plasmons in periodic grids of graphene ribbons: An analytical approach," Phys. Rev. B **94**(19), 195421 (2016).

23. H. Yan, T. Low, W. Zhu, Y. Wu, M. Freitag, X. Li, F. Guinea, P. Avouris, and F. Xia, "Damping pathways of mid-infrared plasmons in graphene nanostructures," Nat. Photonics **7**(5), 394–399 (2013).

24. T. Low, and P. Avouris, "Graphene plasmonics for terahertz to mid-infrared applications," ACS Nano **8**(2), 1086–1101 (2014).

25. B. Ferguson, X. C. Zhang, "Materials for terahertz science and technology," Nat. Mater. **1**(1), 26–33 (2002).

26. W. Zouaghi, M. D. Thomson, K. Rabia, R. Hahn, V. Blank, and H. G. Roskos, "Broadband terahertz spectroscopy: principles, fundamental research and potential for industrial applications," Eur. J. Phys. **34**(6), S179 (2013).

27. J. M. Poumirol, P. Q. Liu, T. M. Slipchenko, A. Y. Nikitin, L. Martin-Moreno, J. Faist, and A. B. Kuzmenko, "Electrically controlled terahertz magneto-optical phenomena in continuous and patterned graphene," Nat. Commun. **8**, (2017).

28. K. E. Peiponen, A. Zeitler, and M. Kuwata-Gonokami, *Terahertz Spectroscopy and Imaging* (Springer-Verlag, 2013).

29. D. Rodrigo, T. Low, D. B. Farmer, H. Altug, and P. Avouris, "Plasmon coupling in extended structures: Graphene superlattice nanoribbon arrays," Phys. Rev. B **93**(12), 125407 (2016).

30. H. Cheng, S. Chen, P. Yu, J. Li, B. Xie, Z. Li, and J. Tian, "Dynamically tunable broadband mid-infrared cross polarization converter based on graphene metamaterial," Appl. Phys. Lett. **103**(22), 223102 (2013).

31. H. Cheng, S. Chen, P. Yu, J. Li, L. Deng, and J. Tian, "Mid-infrared tunable optical polarization converter composed of asymmetric graphene nanocrosses," Opt. Lett. **38**(9), 1567–1569 (2013).

32. H. Cheng, S. Chen, P. Yu, W. Liu, Z. Li, J. Li, B. Xie, and J. Tian, "Dynamically tunable broadband infrared anomalous refraction based on graphene metasurfaces," Adv. Opt. Mater. **3**(12), 1744–1749 (2015).

33. J. Li, P. Yu, H. Cheng, W. Liu, Z. Li, B. Xie, S. Chen, and J. Tian, "Optical polarization encoding using graphene-loaded plasmonic metasurfaces," Adv. Opt. Mater. **4**(1), 91–98 (2016).

34. Y. Li, J. Zhao, H. Lin, W. Milne, and Y. Hao, "Tunable circular polarization selective surfaces for low-THz applications using patterned graphene," Opt. Express **23**(6), 7227–7236 (2015).

35. C. Yang, Y. Luo, J. Guo, Y. Pu, D. He, Y. Jiang, J. Xu, and Z. Liu, "Wideband tunable mid-infrared cross polarization converter using rectangle-shape perforated graphene," Opt. Express **24**(15), 16913–16922 (2016).

36. F. Ling, G. Yao, and J. Yao, "Active tunable plasmonically induced polarization conversion in the THz regime," Sci. Rep. **6**, 34994 (2016).

37. M. Chen, X. F. Xiao, L. Z. Chang, C. Y. Wang, and D. P. Zhao, "High-efficient and multi-frequency polarization converters based on graphene metasurface with twisting double L-shaped unit structure array," Opt. Commun. **394**(1), 50–55 (2017).

38. Q. Bao, H. Zhang, B. Wang, Z. Ni, C. H. Y. X. Lim, Y. Wang, D. Y. Tang, and K. P. Loh, "Broadband graphene polarizer," Nat. Photonics **5**(7), 411–415 (2011).

39. B. Amorim, P. A. D. Goncalves, M. I. Vasilevskiy, and N. M. R. Peres, "Impact of graphene on the polarizability of a neighbour nanoparticle: a dyadic Green's function study," Appl. Sci. **7**(11), 1158 (2017).

40. J. Hao, Y. Yuan, L. Ran, T. Jiang, J. A. Kong, C. T. Chan, and L. Zhou, "Manipulating electromagnetic wave polarizations by anisotropic metamaterials," Phys. Rev. Lett. **99**(6), 063908 (2007).

41. R. M. Roth, N. C. Panoiu, M. M. Adams, J. I. Dadap, and R. M. Osgood, "Polarization-tunable plasmon-enhanced extraordinary transmission through metallic films using asymmetric cruciform apertures," Opt. Lett. **32**(23), 3414–3416 (2007).

42. P. G. Thompson, C. G. Biris, E. J. Osley, O. Gaathon, R. M. Osgood, N. C. Panoiu, and P. A. Warburton, "Polarization-induced tunability of localized surface plasmon resonances in arrays of sub-wavelength cruciform apertures," Opt. Express **19**(25), 25035–25047 (2011).

43. R. Rajkumar, N. Yogesh, and V. Subramanian, "Cross polarization converter formed by rotated-arm-square chiral metamaterial," J. Appl. Phys. **114**(22), 224506 (2013).

44. Y. Zhao and A. Alu, "Tailoring the dispersion of plasmonic nanorods to realize broadband optical metawaveplates," Nano Lett. **13**(3), 1086–1091 (2013).

45. N. K. Grady, J. E. Heyes, D. R. Chowdhury, Y. Zeng, M. T. Reiten, A. K. Azad, A. J. Taylor, D. A. Dalvit, and H. T. Chen, "Terahertz metamaterials for linear polarization conversion and anomalous refraction," Science **16**, 1235399 (2013).

46. L. Li, T. Li, X. M. Tang, S. M. Wang, Q. J. Wang, and S. N. Zhu, "Plasmonic polarization generator in well-routed

beaming," Light Sci. Appl. **4**(9), e330 (2015).

47. W. Wang, Z. Guo, R. Li, J. Zhang, A. Zhang, Y. Li, Y. Liu, X. Wang, and S. Qu, "L-shaped metasurface for both the linear and circular polarization conversions," J. Optics **17**(6), 065103 (2015).

48. Q. Guo, C. Schlickriede, D. Wang, H. Liu, Y. Xiang, T. Zentgraf, and S. Zhang, "Manipulation of vector beam polarization with geometric metasurfaces," Opt. Express **25**(13), 14300–14307 (2017).

49. X. J. Shang, X. Zhai, J. Yue, X. Luo, J. P. Liu, X. P. Zhu, H. G. Duan, and L. L. Wang, "Broad-band and high-efficiency polarization converters around 1550 nm based on composite structures," Opt. Express **25**(13), 14406–14413 (2017).

50. M. R. Querry, "Optical constants," Contractor Report **415**, (1985).

51. A. Taflove and S. C. Hagness, *Computational Electrodynamics: The Finite-Difference Time-Domain Method* (Artech House, 2005).

52. J. W. You and N. C. Panoiu are preparing a manuscript to be called "Computational analysis of dispersive and nonlinear 2D materials by using a novel GS-FDTD method."

53. J. A. Kong, *Electromagnetic wave theory* (EMW Publishing, Massachusetts, 2008).

---

1. Introduction

Graphene, an atomic-layer thin material [1], exhibits many unique and remarkable physical properties, including high carrier mobility [2], chemical stability, and high mechanical strength, which has led to intense research interest in science and engineering. In particular, its linear optical properties have been employed in many photonics and optoelectronics applications [3, 4], including novel electronic devices [5–7], sensors [8], and solar cells [9]. In addition to the impact of graphene on the field of linear optics, its nonlinear optical properties have played an equally important role in the development of novel active photonic devices with new or improved functionality. Specifically, nonlinear optical interactions, such as third-harmonic generation (THG) [10–13] and Kerr effect [14], which are key for many active photonic devices [15], are strongly enhanced in graphene nanostructures because these physical systems support surface plasmon-polaritons (SPPs) that strongly confine and enhance the optical near-field.

Because of the specific optical properties of graphene [16, 17], most of its applications are found in the THz frequency domain. In particular, the conductivity of graphene at THz frequencies is determined by intra-band transitions [18–20], namely its dispersive properties are similar to those of noble metals described by the Drude model. For this reason, graphene structures can support broadband plasmon resonances in the THz and mid-IR regime, which can be used to enhance and control the optical near-field. Moreover, the size of patterned graphene structures with resonances in the THz domain is about two orders of magnitude smaller than that of metallic structures whose resonances are at similar frequencies, which underlines the potential for miniaturization provided by graphene structures [21–24]. Equally important, due to the tunability of graphene, plasmon resonance frequencies can be ultrafast tuned via chemical or electrical doping.

In addition to many other THz applications [25–29], the optical properties of graphene make it particularly suitable to be employed in an important class of THz devices, namely polarization converters. Although the THz technology for generation and control of light polarization is still in its infancy, recently significant progress has been made in this area of research. Thus, several designs of graphene based polarization converters operating in transmission or reflection have been proposed and used to demonstrate the conversion of the polarization state of light from linearly polarized to a different linearly polarized state or to right- and left-circularly polarized (RCP, LCP) light [30–39]. In addition, polarization converters based on metallic structures have also been demonstrated [40–49], although they are bulkier and have a significantly larger size as compared to similar devices based on graphene. Despite this recent progress, a key functionality still has to be implemented in reliable devices, namely tunable and ultrafast controllable THz polarization converters.

In order to address this problem, in this paper we demonstrate that graphene nanostructures can be used effectively both to convert THz light between different polarization states and to generate optical waves at new frequencies and with pre-designed polarization states. The proposed structures consist of two crossed graphene gratings, which are separated by an insulator

spacer. These ultra-thin graphene optical metasurfaces can be utilized as polarization converters to engineer and control the polarization state of THz waves simply by choosing the specific geometrical properties of the two crossed gratings or by tuning the optical properties of graphene by varying its conductivity. Our analysis shows that these graphene based polarizaion converters can be very effective in generating specific polarization states, including linearly polarized, RCP, LCP, and elliptically polarized THz waves.

The paper is organized as follows. In Sec. 2, the linear and nonlinear properties of graphene are briefly summarized and in Sec. 3, the THz response of a crossed graphene grating configuration is investigated. We then illustrate in Sec. 4 and Sec. 5 how these ideas can be used to design polarization converters that can be employed in the linear regime and at higher harmonics, respectively. The main conclusions of the paper are summarized in the last section.

2. Linear and Nonlinear Optical Properties of Graphene

The linear optical properties of graphene are described by its linear surface conductivity, which is given by the Kubo's formula [16, 17]. Within the random-phase approximation, this formula can be expressed as the sum of the inter-band and the intra-band contributions. The intra-band contribution is given by

$$\sigma_{intra}(\omega, \mu_c, \tau, T) = -\frac{ie^2 k_B T}{\pi \hbar^2 (\omega - i\tau^{-1})} \left[\frac{\mu_c}{k_B T} + 2 \ln \left(e^{-\frac{\mu_c}{k_B T}} + 1 \right) \right], \tag{1}$$

where, ω is the angular frequency, μ_c is the chemical potential, τ is the relaxation time, T is the temperature, e indicates the electron charge, k_B is the Boltzmann constant, and $\hbar$ represents the reduced Planck's constant. Moreover, if $\mu_c \gg k_B T$ and $\hbar \omega \ll 2\mu_c$, the inter-band contribution can be approximated as

$$\sigma_{inter}(\omega, \mu_c, \tau, T) = -\frac{ie^2}{4\pi \hbar} \ln \left[\frac{2|\mu_c| - (\omega - i\tau^{-1})\hbar}{2|\mu_c| + (\omega - i\tau^{-1})\hbar} \right]. \tag{2}$$

It can be seen that the intra-band contribution to the conductivity of graphene at THz frequencies is similar to that of noble metals, meaning that it is described by the Drude model. This linear property indicates that graphene can support plasmon resonances at THz frequencies.

The nonlinear optical properties of graphene are quantified by a nonlinear surface conductivity tensor, $\sigma_s^{(m)}(\Omega, \omega)$, where the superscript m indicates the order of the nonlinear optical interaction and Ω is the frequency of the higher harmonic. The graphene lattice is centrosymmetric, which means that second-order nonlinear optical processes are forbidden. Thus, in this paper we only consider the third-harmonic generation, namely $m = 3$ and the conductivity tensor is described by a single scalar function. This function can be written as [10–12]:

$$\sigma_s^{(3)}(\Omega, \omega) = -\frac{i\sigma_0(\hbar v_F e)^2}{48\pi(\hbar\omega)^2} T \left(\frac{\hbar\omega}{2|\mu_c|} \right), \tag{3}$$

where $\Omega = 3\omega$, $v_F \approx c/300$ is the Fermi velocity, $\sigma_0 = e^2/4\hbar$ is the universal dynamic conductivity of graphene, and $T(x) = 17G(x) - 64G(2x) + 45G(3x)$, with $G(x) = \ln \left| \frac{1+x}{1-x} \right| - i\pi H(|x|-1)$ and $H(\cdot)$ being the Heaviside step function. Using the third-order surface conductivity tensor of graphene [12], the corresponding current density can be calculated as:

$$J_{d,i}^{(3)}(\Omega, \omega) = \sigma_s^{(3)}(\Omega, \omega) \sum_{j,k,l=1}^{3} \Delta_{ijkl}^{(3)} E_j(\omega) E_k(\omega) E_l(\omega), \tag{4}$$

where $\Delta_{ijkl}^{(3)} = (\delta_{ij}\delta_{kl} + \delta_{ik}\delta_{jl} + \delta_{il}\delta_{jk})/(3h_{eff})$, h_{eff} being the effective thickness of graphene and δ_{ij} the Kronecker delta. In 2D materials, the nonlinear surface current lies on the surface, thus the value of the normal component of the current density in Eq. (4) is zero.

3. Crossed Graphene Polarizer

The material and geometrical structure of the investigated device is schematically illustrated in Fig. 1. It consists of three layers, namely two optical gratings made of graphene nanoribbons (GNRs) separated by a dielectric thin film assumed to be made of Al_2O_3, the whole structure being placed on a silicon substrate. In particular, the two sets of GNRs are oriented perpendicular to each other so that they couple to plane waves with different (orthogonal) polarizations. In addition, metallic electrodes are in contact to the two graphene gratings so that one can tune the Fermi energy of graphene and implicitly its linear and nonlinear conductivities. The unit cell of this crossed GNRs-insulator-GNRs (GIG) metasurface is depicted in the inset of Fig. 1, the metasurface being described by the periods L_1 and L_2, thickness of the dielectric spacer, d, and the widths of the bottom and the top ribbons, W_1 and W_2, respectively.

In our computational analysis of the optical response of this crossed graphene polarizer, we assume that a linearly polarized THz optical wave carrying a modulated Gaussian pulse is impinging normally onto the metasurface, as shown in Fig. 1. The frequency band of this Gaussian pulse ranges from 3 THz to 10 THz and the polarization of the incident plane wave is characterized by the polarization angle, α. In this work, unless otherwise specified, the parameters defining the GIG metasurface are: $d = 100$ nm, $L_1 = L_2 = 200$ nm, and $W_1 = W_2 = 150$ nm. Moreover, the refractive index of Al_2O_3 and silicon are taken from [50], and the linear conductivity of graphene is given by Eqs. (1)–(2) with $T = 300$ K, $\tau = 0.2$ ps, and $\mu_c = 0.2$ eV. The linear response of this device is studied using the ADE-FDTD method [51], whereas its nonlinear optical properties are investigated using a numerical method we introduced in a recent study [52].

In order to understand the basic optical properties of the GIG polarizer, we determined first its linear optical response, namely the reflectance, R, transmittance, T, and absorption, A. The results of this analysis, summarized in Fig. 2, reveal several important features. First, as mentioned above, due to its metallic character graphene supports surface plasmons. Their signature can be seen in the reflectance and absorption spectra plotted in Fig. 2 as broad spectral peaks. These
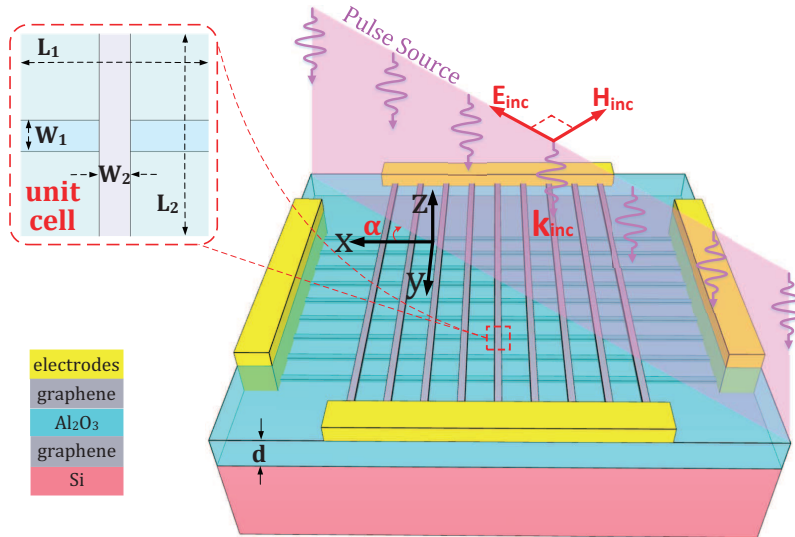

Fig. 1. Schematics of a crossed graphene polarizer consisting of two optical gratings made of graphene nanoribbons separated by a dielectric thin film. The polarization angle of the incident light is α, and one unit cell of this metasurface with periods L_1 and L_2 is depicted in the inset. The widths of the graphene nanoribbons of the top and bottom gratings are W_1 and W_2, respectively.
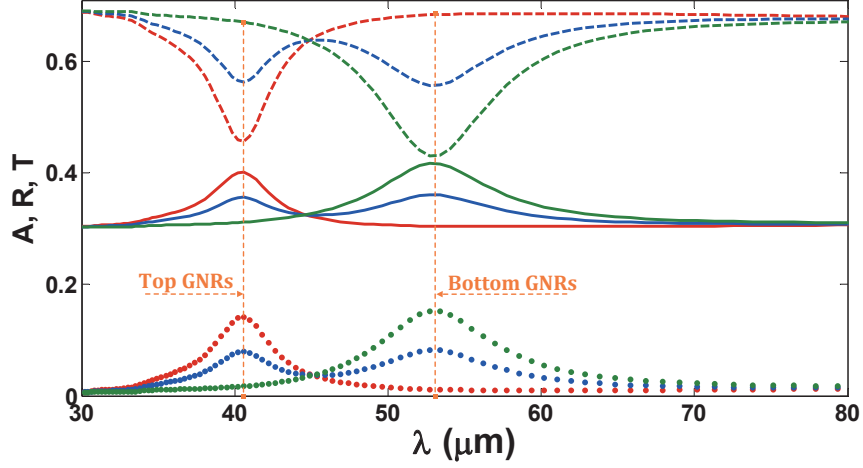
Fig. 2. Linear spectra of absorption (*A*, dotted line), reflectance (*R*, continuous line), and transmittance (*T*, dashed line) of a crossed graphene polarizer, calculated for three values of the incidence polarization angle: $\alpha = 0$ (red lines), $\alpha = \pi/4$ (blue lines), and $\alpha = \pi/2$ (green lines). The values of all the geometrical and material parameters of the structure are provided in the text.

plasmon resonances are generated when the electric field of the incident wave is perpendicular to the GNRs (TM polarization). Moreover, the enhanced absorption at the resonance wavelengths as well as the optical near-field (not shown here) suggest that the excitation of these plasmons is accompanied by a strong enhancement of the local optical field. Equally important, the resonance wavelengths can be tuned significantly simply by varying the Fermi energy of graphene.

Another important and somewhat surprising fact illustrated by the spectra in Fig. 2 is that the resonances corresponding to the top and bottom GNRs are located at different wavelengths, despite the fact that the top and bottom graphene gratings are identical ($W_1 = W_2$ and $L_1 = L_2$). This result is explained by the fact that the two gratings are embedded in a different electromagnetic environment, namely the top one is located in-between an air region and the Al_2O_3 spacer whereas the bottom one is sandwiched in-between the Al_2O_3 spacer and silicon substrate. To be more specific, the resonance wavelength of graphene plasmons is particularly sensitive to the permittivity of the environment. For example, the dispersion relation of plasmons in a graphene sheet sandwiched in-between two media with permittivities ϵ_1 and ϵ_2 is [17]:

$$k_{sp} \approx \frac{\pi\hbar^2}{e^2\mu_c}(\epsilon_1 + \epsilon_2)\omega(\omega + i\tau^{-1}), \tag{5}$$

where k_{sp} is the plasmon wavenumber. This relation suggests that the larger the permittivity is the larger the resonance wavelength of the plasmons of GNRs is. This can be observed in Fig. 2, where the resonance wavelength of the plasmons of the bottom GNRs is larger than that of the top GNRs because the permittivity of silicon is much larger than that of air. In other words, the peak corresponding to the larger resonance wavelength (53 μm) arises from the excitation of plasmons in the bottom GNRs, whereas the plasmons of the top GNRs give rise to the peak at the smaller resonance wavelength (41 μm).

In contrast to metallic plasmon resonances, which are solely determined by the geometry, graphene plasmons can be readily controlled in real-time via a gate voltage. Moreover, the polarization-dependent optical response of the proposed crossed graphene gratings can be used to effectively reduce the size of commonly used metal based THz polarizers. In order to illustrate
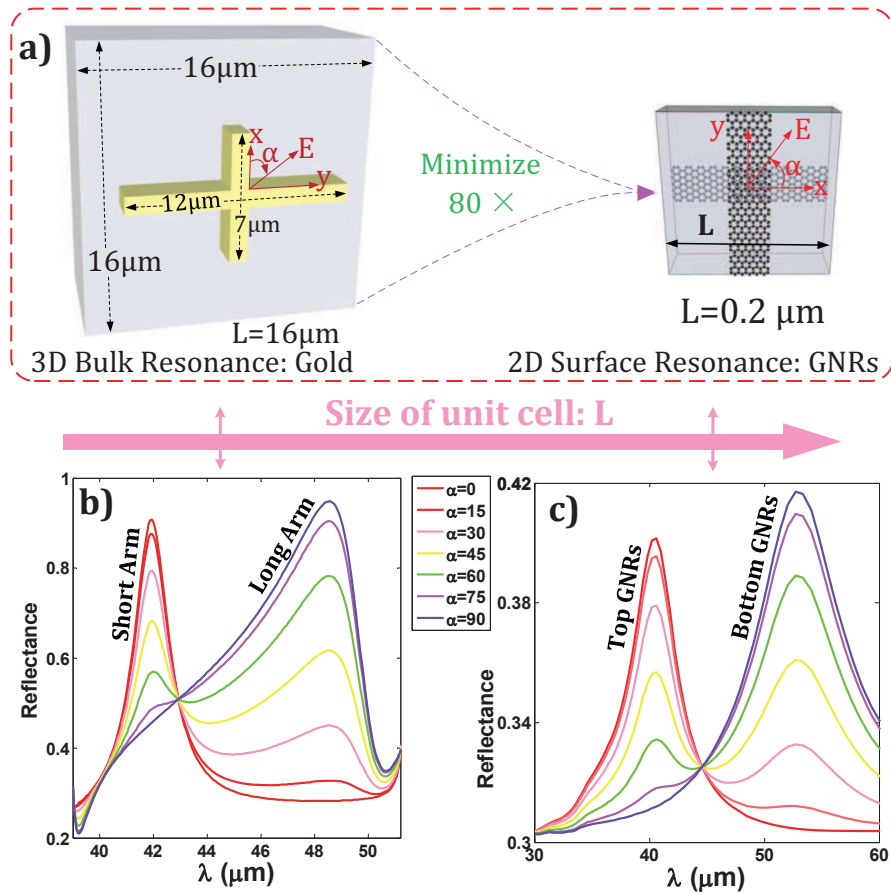
Fig. 3. a), b) Schematics of the unit cell of a polarizer based on metal and graphene, respectively. c), d) Reflectance spectra of metal and graphene based polarizers, respectively, determined for different polarization angles of the incident wave.

this idea, we consider two polarizers, one made of graphene and the other one of gold, and determine their size such that both have plasmon resonances at similar wavelengths. In the case of the metallic polarizer, we use a widely investigated structure, namely an asymmetric cruciform particle with the lengths of the two arms $L_1 = 7\,\mu m$ and $L_2 = 12\,\mu m$, the periods of the structure being $L_x = L_y \equiv L = 16\,\mu m$. As illustrated in Fig. 3, the metallic and graphene polarizers have resonances at similar wavelengths if the corresponding sizes of their unit cell are $L = 16\,\mu m$ and $L = 0.2\,\mu m$, respectively. Note that in the case of the metallic polarizer the two resonances correspond to different wavelengths because the two arms of the cross have different length. More specifically, plasmons are excited in an arm of the cross when the incident field is parallel to the arm, and the corresponding resonance wavelength increases when the length of the arm increases. This analysis proves that by employing graphene based polarizers the size of the device can be reduced by almost two orders of magnitude as compared to that of conventional, metal based devices. It should be noted that the maximum reflectivity and bandwidth of crossed GNR gratings do not favorable compare to those of similar structures made of crossed metallic gratings. On the other hand, the photonic structures analyzed in our work do have important advantages, such as a significantly reduced size.

4. Polarization Converter Based on Crossed Graphene Polarizer

As we discussed in the preceding section, the polarization-selective feature of a GIG metasurface can be used to design an efficient, ultrathin polarization converter. In this section, such a polarization converter based on the linear optical properties properties of graphene is presented and studied. The schematics of this device is shown in Fig. 4(a). Similarly to the polarizer presented in Fig. 1, the proposed polarization converter consists of two crossed graphene gratings, which are placed on the top and at the bottom of an insulator spacer made in this case of PMMA. The size of the unit cell of this graphene polarization converter is the same as that of the polarization polarizer in Fig. 1. We chose this modified structure of the device to ensure that the two graphene gratings are sandwiched in-between the same pair of optical media, and so the corresponding resonance wavelengths of the plasmons are the same. This does not affect the generality of the conclusions of our study, yet it simplifies the device analysis. It should also be noted that part of the incident beam will be reflected if the two graphene gratings are sandwiched in-between different media. However, the influence of the reflection from the substrate can be effectively removed if one uses two independent simulations or experiments, namely one with just the substrate and the other one with the GNRs on top of the substrate, and then properly subtract the two simulated or measured reflected beams.

We consider first the transmittance, reflectance, and absorption of a single graphene grating placed on top of a PMMA substrate, the corresponding spectra calculated for the polarization angle $\alpha = 0$, $\alpha = \pi/4$, and $\alpha = \pi/2$ being presented in Fig. 4(b). These spectra show that when the electric field is parallel to the GNRs, the transmittance is almost unity whereas the reflectance is zero. On the other hand, when the field is polarized perpendicularly to the GNRs, at the resonance wavelength of the plasmon $T \simeq 50\%$ and $R \simeq 10\%$.

The linear optical response of the graphene polarization converter, that is the transmittance, reflectance, and absorption spectra, is also given in Fig. 4(b). Because of the symmetry of the structure, all optical spectra are polarization independent. In particular, the resonance wavelength
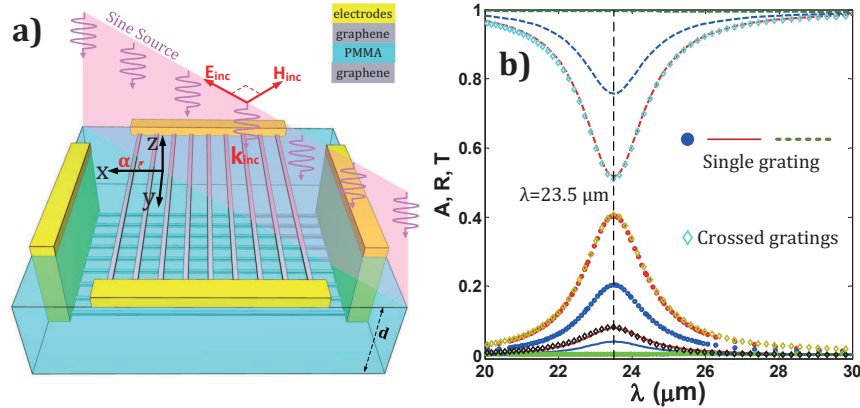

Fig. 4. a) Schematics of a crossed graphene polarizer consisting of two optical gratings made of graphene nanoribbons separated by a thin film made of PMMA. The values of the geometrical parameters of the structure and all material parameters are provided in the text. (b) Linear spectra of absorption (A, dotted line), reflectance (R, continuous line), and transmittance (T, dashed line) corresponding to a graphene grating placed on top of PMMA substrate, calculated for three values of the incidence polarization angle: $\alpha = 0$ (red lines), $\alpha = \pi/4$ (blue lines), and $\alpha = \pi/2$ (green lines). The spectra marked with diamond symbols show A (citron), R (black), and T (light blue) of the crossed-grating structure and are calculated for $\alpha = \pi/4$.
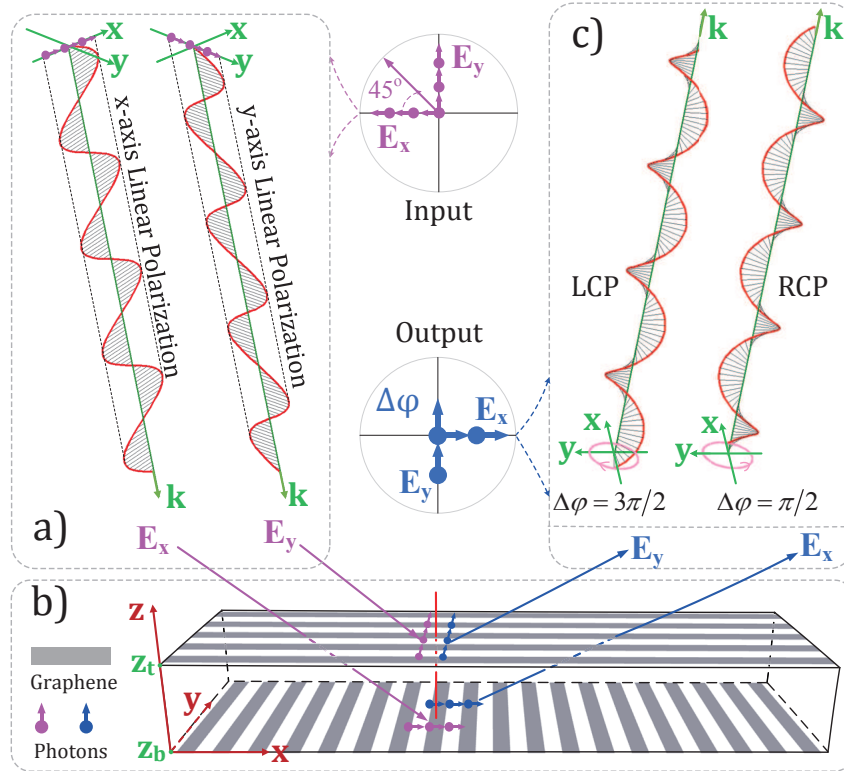
Fig. 5. Configuration of a crossed-graphene grating that can be used as a polarization converter in reflection. a) An incident linearly polarized beam with polarization angle $\alpha = \pi/4$ impinges normally on a crossed-graphene grating, such that the E_x and E_y field components interact primarily with the bottom and top grating, respectively. b) Schematics of the crossed-graphene grating. c) Depending on the value of the phase difference $\Delta\varphi$, one can engineer reflected optical beams with desired polarization state.

of the plasmons supported by the two graphene gratings does not depend on the polarization angle of the incident wave; however, both the spectra and the resonance wavelength can be tuned by changing the Fermi energy of graphene.

The operation principles of the proposed polarization converter, designed to operate in reflection, are illustrated in Fig. 5. Thus, let us assume that a linearly polarized incident wave with a polarization angle $\alpha = 45°$ impinges normally onto the top facet of the device. The incoming field is decomposed along the x-axis and y-axis, that is, along the directions of the GNRs in the bottom and top graphene gratings, respectively. Based on the polarization-selective property of graphene gratings, illustrated in Fig. 4(b), the E_y field component will pass largely unaffected through the top graphene grating, will propagate through the spacer to the bottom grating, where part of it will be reflected. Then, it will propagate back to the top grating and pass through it largely without being affected. The E_x field component, on the other hand, will be reflected by the top graphene grating. This simple analysis suggests that there will be an optical phase difference, $\Delta\varphi$, between the phases of the reflected E_x and E_y field components, meaning that upon reflection from the polarization converter the linearly polarized incident optical field would be generally converted into an elliptically polarized one. More specifically, by tuning $\Delta\varphi$, one can engineer output waves with a specific state of polarization, including linearly polarized, RCP, and LCP optical beams.

Let us now derive an expression for the phase difference $\Delta\varphi$. Whereas a rigorous analytical formula for $\Delta\varphi$ cannot be determined, due to the fact that the optical field in the region of the two graphene gratings is strongly inhomogeneous, a simple formula can be derived under the following assumptions: *i)* The fields in the transmission region, spacer, and reflection region can be represented as superposition of plane waves and *ii)* The E_y field component undergoes a single reflection at the interface containing the bottom grating. Under these conditions, a simple analysis of the wave configuration depicted in Fig. 5 shows that $\Delta\varphi$ is given by the following relation:

$$\Delta\varphi(z) = \begin{cases} 0, & z < z_b, \\ \frac{4\pi n}{\lambda}(z - z_b), & z_b < z < z_t, \\ \frac{4\pi n}{\lambda}d, & z > z_t, \end{cases} \tag{6}$$

where z_b and z_t indicate the location of the bottom and top graphene gratings, respectively, n is the index of refraction of the spacer, and d is its thickness. This equation shows that $\Delta\varphi$ is constant in the transmission and reflection regions, and increases linearly with z in the spacer.

Equation (6) can be used to design a polarization converter that generates an optical beam with a desired polarization state. In particular, if $\Delta\varphi(d) = l\pi$, where l is an integer, the output beam will be linearly polarized, if $\Delta\varphi(d) = (4l + 1)\pi/2$ $[\Delta\varphi(d) = (4l + 3)\pi/2]$ the output beam will be RCP (LCP), whereas for other values of $\Delta\varphi(d)$ the output beam will be elliptically polarized. The phase difference $\Delta\varphi$ can be varied simply by changing the thickness d of the dielectric spacer.

In order to assess how well Eq. (6) describes the dependence of $\Delta\varphi$ on distance, we computed numerically this phase difference and compared the results with the analytical predictions based on Eq. (6). These calculations were performed for an incident beam with $\lambda = 23.5\,\mu m$, that is at the plasmon resonance shown in Fig. 4(b). The conclusions of this analysis are summarized in Fig. 6(a). It can be seen that there is a very good agreement between the analytical and numerical results, especially away from the interfaces where the two graphene gratings are located. In these two regions, the phase difference $\Delta\varphi(z)$ shows strong spatial inhomogeneity, which is attributable to the strong near-field confinement of the graphene plasmons. Interestingly enough, the phase variations at the two interfaces containing the graphene gratings have identical absolute
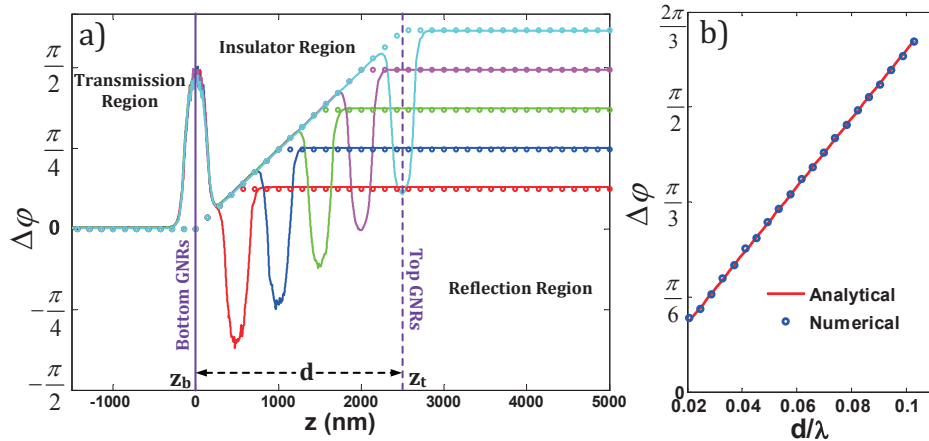

Fig. 6. a) Dependence of the linear phase difference $\Delta\varphi$ on z, determined for different values of the thickness of the insulator layer: $d = 0.5\,\mu m$ (red line), $d = 1\,\mu m$ (blue line), $d = 1.5\,\mu m$ (green line), $d = 2\,\mu m$ (purple line), and $d = 2.5\,\mu m$ (cyan line). The solid lines and circles indicate the numerical and analytical results, respectively. b) Phase difference $\Delta\varphi$ vs. the ratio d/λ, determined analytically and numerically in the reflection region. In all calculations $\lambda = 23.5\,\mu m$ corresponds to the plasmon resonance shown in Fig. 4(b).

values but are opposite in sign. As a result, they cancel each other, which results in a constant phase difference in the transmission and reflection regions. Moreover, the numerically obtained $\Delta\varphi(z)$, presented in Fig. 6(a), validates our assumption that the optical field in the transmission, reflection, and spacer regions can be represented as superpositions of plane waves.

As Eq. (6) and our calculations indicate, a specific polarization state of the output beam can be achieved by carefully choosing the the thickness of the spacer or the wavelength of the input beam. In order to illustrate this idea, we show in Fig. 6(b) the dependence of $\Delta\varphi$ on the ratio d/λ, determined both analytically and numerically. In these calculations, we again set the wavelength to be equal to the wavelength of the plasmon resonance shown in Fig. 4(b), *i.e.* $\lambda = 23.5\,\mu m$. This analysis further validates Eq. (6), as it shows a very good agreement between theoretical predictions and computational results. Moreover, Fig. 6(b) suggests that our polarization converter is particularly compact, that is large phase variations can be achieved for a relatively small thickness, d. For example, in order to transform the linearly polarized input beam into a RCP beam, *i.e.* $\Delta\varphi = \pi/2$, the thickness is $d \simeq 0.1\lambda$.

5. Active Polarization Converter Based on Crossed Graphene Polarizer

One important functionality of the polarization converter analyzed in the preceding section is that it can be used as an active device, too, namely it can generate optical beams at higher-harmonics with specific polarization state. Whereas our analysis of the nonlinear properties of this device is valid for any order of the nonlinearity, we consider in this paper only THG, namely the order of the nonlinear optical interaction is $m = 3$.

Arguments similar to those used to derive Eq. (6) can be employed to find the corresponding formula valid in the nonlinear case. The conclusion of this analysis is that in the nonlinear case the nonlinear phase difference $\Delta\varphi$ is described by a relation very similar to Eq. (6), the only modification being that the wavelength λ must be replaced by $\lambda \rightarrow \Lambda = \lambda/m$, where $\Lambda = \lambda/m = \lambda/3$ is the wavelength at the third-harmonic (TH). For example, for $z > z_t$, the nonlinear phase difference can be written as $\Delta\varphi = \Delta\varphi_1 + \Delta\varphi_2$, where $\Delta\varphi_1 = \Omega\Delta t = \Omega n d/c$ accounts for the fact that there is a $\Delta t = nd/c$ time delay between the TH waves generated at the top and bottom graphene gratings and $\Delta\varphi_2 = Knd$, with $K = 2\pi/\Lambda$ being the wave vector at the
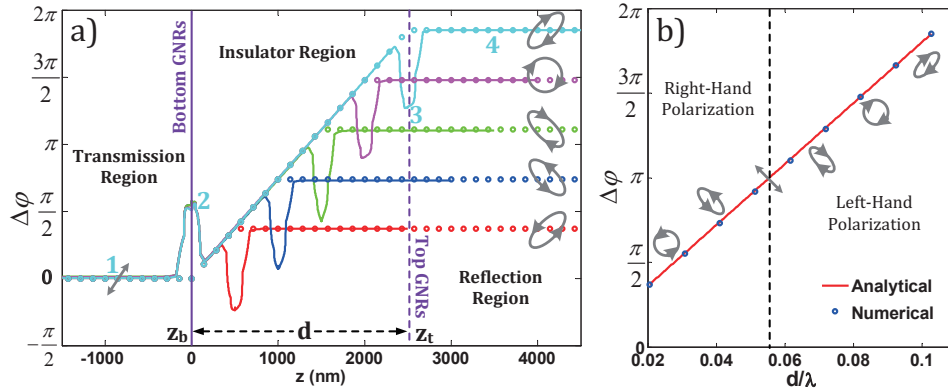

Fig. 7. a) Dependence of the nonlinear phase difference $\Delta\varphi$ on z, determined for different values of the thickness of the insulator layer: $d = 0.5\,\mu m$ (red line), $d = 1\,\mu m$ (blue line), $d = 1.5\,\mu m$ (green line), $d = 2\,\mu m$ (purple line), and $d = 2.5\,\mu m$ (cyan line). The solid lines and circles indicate the numerical and analytical results, respectively. b) Phase difference $\Delta\varphi$ vs. the ratio d/λ, determined analytically and numerically in the reflection region. In all calculations $\lambda = 23.5\,\mu m$ corresponds to the plasmon resonance shown in Fig. 4(b).

TH, is the phase variation at the TH of the reflected wave propagating from the bottom to the top graphene grating. Adding the two phases leads to $\Delta\varphi = 4\pi n d/\Lambda$.

As in the linear case, we determined the phase difference $\Delta\varphi$ using Eq. (6), modified as just discussed, and numerically by employing an in-house developed code that implements the GS-FDTD method [52]. In order to be able to compare these results to those obtained in the linear case, we use the same value of the wavelength of the incident wave, $\lambda = 23.5\,\mu m$. The conclusions of these investigations, summarized in Fig. 7, show that in the nonlinear case, too, there is a good agreement between the theoretical and computational results, except within a small region near the graphene gratings. In these regions the nonlinear optical field is strongly distorted from a plane wave, as the nonlinear currents, which are the sources for the field at the TH, lie on the GNRs. Moreover, it can be seen in in Fig. 7(b), that the nonlinear phase difference is larger by a factor of $m = 3$ than the linear one, which leads to a more compact device. More specifically, $\Delta\varphi$ varies from 0 to 2π when the ratio d/λ varies from 0 to 0.116, which means that a linearly polarized incident wave is converted at the TH into a right-hand elliptically polarized optical wave when $d/\lambda < 0.058$ and into a left-hand elliptically polarized optical wave when $0.058 < d/\lambda < 0.116$.

A facile and intuitive representation of the polarization state of an optical beam is based on the Stokes parameters, Q, U, and V, and the corresponding Poincaré sphere [53]. Using these tools, we mapped the z-dependence of the nonlinear phase difference $\Delta\varphi(z)$ for the cases presented in Fig. 7(a) onto the Poincaré sphere, the results being presented in Fig. 8. Thus, each point on these paths on the Poincaré sphere represents a specific polarization state corresponding to a value of the z-coordinate. For instance, the points located on the equator represent linearly polarized waves, and the points located in the northern and southern hemispheres represent right-hand and left-hand elliptically polarized waves, respectively. The particular cases of circularly polarized waves are located at the two poles.

Let us consider first the case presented in Fig. 8(a), which corresponds to a polarization converter designed to transform a linearly polarized plane wave into a RCP optical beam at the TH. In this and all the other cases, the initial state of polarization corresponds to the point 1 on the Poincaré sphere because the initial value of the phase difference is zero. Note that $\Delta\varphi = 0$ in
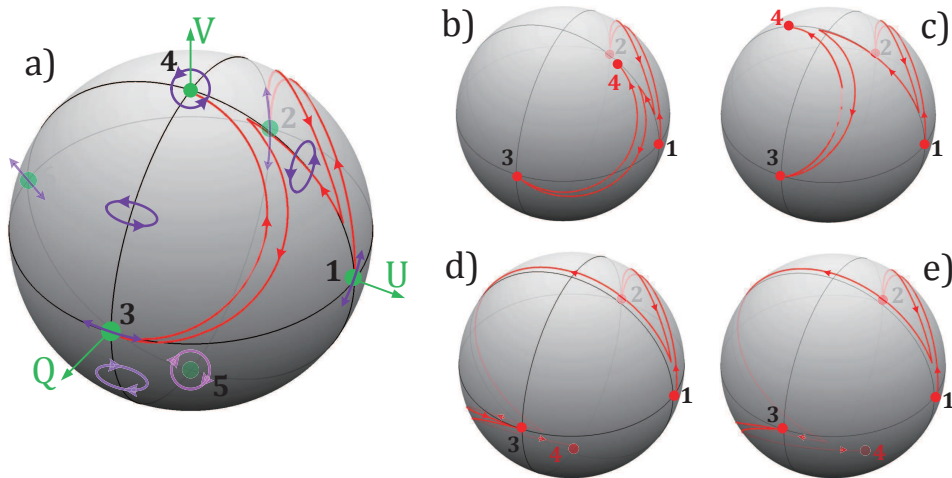

Fig. 8. Representation on the Poincaré sphere of polarization states described by the nonlinear phase difference $\Delta\varphi(z)$. a) Poincaré sphere and the polarization transformation path (red line) when $d = 0.8\,\mu m$. b), c), d), e) Polarization transformation paths (red lines) corresponding to $d = 0.5\,\mu m$, $d = 1\,\mu m$, $d = 2\,\mu m$, and $d = 2.5\,\mu m$, respectively.

the transmission region ($z < 0$), too, so that the transmitted TH optical beam corresponds to the point *1*, too. Moreover, it can be seen in Fig. 8 that all polarization paths pass through the points *2* and *3*, which correspond to the bottom ($z = z_b$) and top ($z = z_t$) graphene gratings, respectively. In order to understand this fact, note that the bottom graphene grating is primarily excited by an *x*-polarized field, and therefore the generated field at the TH is *x*-polarized, too. As a result, the field at $z = z_b$ is mapped to the point *2* on the Poincaré sphere. Following a similar argument it can be shown the field at the top graphene grating is *y*-polarized, so that the field at $z = z_t$ is mapped to the point *3* on the Poincaré sphere.

The location on the Poincaré sphere of the end point, *4*, of the polarization state depends on the thickness *d*, as the phase difference at $z = z_t$ is proportional to *d*. This is illustrated in Figs. 8(b) through 8(e), which correspond to increasing values of *d*. Considering this feature, we can engineer the thickness *d* so as the end point of the polarization path corresponds to a desired polarization state. For instance, as shown in Fig. 8(a), when the thickness $d = 0.8\,\mu$m, the polarization path ends at the north pole, which corresponds to a RCP optical beam at the TH.

6. Conclusions

In summary, we have introduced and discussed the operation principles and optical properties of an ultrathin graphene polarizer and a novel graphene polarization converter based on crossed graphene optical gratings. These photonic devices are designed to operate at THz frequencies and are based on the unique linear and nonlinear optical properties of graphene nanoribbons. In particular, our study demonstrates that graphene nanoribbons can support strong plasmon resonances at THz frequencies, a feature that can be used to reduce the device size by more than 80 times, as compared to metallic devices with similar structure. Moreover, we also show that the polarization-selective properties of graphene nanoribbon gratings can be effectively employed to design passive and active ultrathin graphene polarization converters. In order to characterize the performance of this novel type of polarization converters, we have derived an analytical model, validated by rigorous numerical simulations, which describes the polarization state of the reflected optical beams, at both the fundamental frequency and higher-harmonics. Both the analytical and numerical results demonstrate that a linearly polarized incident wave can be converted into an optical beam with desired polarization state, both at the fundamental frequency and higher-harmonics, simply by engineering the geometrical and material parameters defining the proposed graphene polarization converter. Important from a practical perspective, our analysis suggests that the thickness of this novel polarization converter can be as small as 10 % of the wavelength of the incident optical beam.